# 2004年新潟県中越地震により発生した斜面災害について

AUTHOR(S):

佐々, 恭二; 福岡, 浩; 汪, 発武; 王, 功輝; 岡田, 憲治; 丸井, 英明

CITATION:

佐々, 恭二 ...[et al]. 2004年新潟県中越地震により発生した斜面災害について. 京都大学防災研究所年報. C 2006, 49(C): 119-136

ISSUE DATE:

2006-04-01

URL:

http://hdl.handle.net/2433/26680

京都大学防災研究所年報 第 49 号 C 平成 18 年 4 月
Annuals of Disas. Prev. Res. Inst., Kyoto Univ., No. 49 C, 2006

# Landslide Disasters Triggered by the 2004 Mid-Niigata Prefecture Earthquake in Japan

Kyoji SASSA, Hiroshi FUKUOKA, Fawu WANG,
Gonghui WANG, Kenji OKADA*, Hideaki MARUI**

* Japan Meteorological Agency
** Research Center for Natural Hazard and Disaster Recovery, Niigata University, Japan

**Synopsis**

During the 2004 Mid-Niigata Prefecture earthquake, thousands of landslides were triggered. Among them five catastrophic landslides were introduced in this paper. In addition, the influence of rainfalls in prior to the earthquake and the urgent response to prevent disastrous failure of landslide dams were also discussed and presented. Higashi Takezawa and Terano landslides occurred within past landslide masses and dammed the river at the toe of the landslides, causing great damages to the properties. Detailed field investigation was performed on these two landslides. To examine the triggering and movement mechanisms, samples were taken from these landslides. By using a ring shear apparatus, real earthquake wave loading test and cyclic loading tests were performed on these samples. The test results revealed that those sand samples from both landslides can suffer from sliding surface liquefaction phenomenon with very lower final apparent friction angles, while the silt sample from Terano landslide showed no liquefaction failure, indicating that landsliding during this earthquake time was triggered within the sand layer above the silt layer in the past landslide masses. Finally, the movement of Higashi Takezawa landslide was simulated.

**Keywords:** landslide, earthquake, soil water index, ring-shear test, simulation, disaster recovery

## 1. Introduction

The M6.8 Mid-Niigata Prefecture earthquake, occurred at an epicentral depth of 13 km near Ojiya city in Niigata Prefecture at 17:56 on 23 October 2004. 362 landslides with widths of more than 50 m and 12 large-scale landslides with individual volumes of more than 1 million cubic meters were triggered by this earthquake (Ministry of Land, Infrastructure and Transport 2005). It was the greatest earthquake disaster in Japan after the 1995 Hyogoken-Nambu earthquake (M7.2). Mostly, the landslides were reactivation of past large-scale landslide masses. Forty five landslide dams were formed by this earthquake. Within those, five

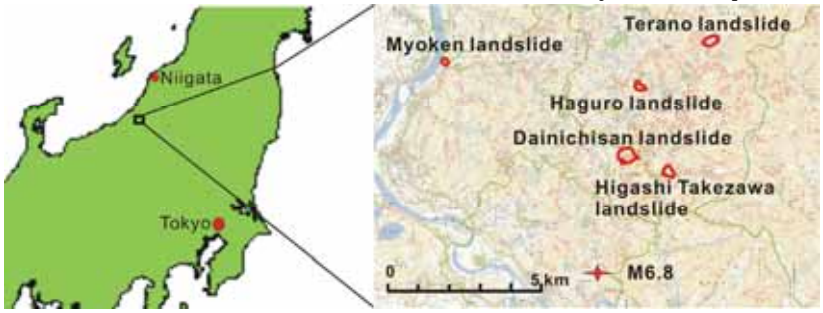


Fig. 1 Locations of the four major landslides triggered by the M6.8 Mid-Niigata Prefecture earthquake


Fig. 2 General view of the Higashi Takezawa landslide. (a) Oblique airphoto taken by Marui on 3 November 2004, (b) Oblique airphoto taken by Sassa on 6 November 2004, (c) Debris intruded into a school building from the landslide mass, d) Side view of the Higashi Takezawa landslide taken on 16 November 2004.

major landslides occurred on Higashi Takezawa, Terano, Dainichisan, Haguro, and Myoken areas (Fig. 1) were the most catastrophic. The Higashi Takezawa landslide and the Terano landslide which formed landslide dams more than 25 m high were investigated in detail. This research presents the dynamic properties of these landslides and the mechanism of large-scale rapid landslides induced by earthquake within past landslide masses, as well as the landsliding computer simulation for the Higashi Takezawa landslide.

## 2. Major landslides triggered by the 2004 Mid-Niigata Prefecture earthquake

The landslide that posed the greatest threat to the area was the Higashi Takezawa landslide, which blocked the Imokawa River, forming a landslide dam. Fig. 2a, b show the general view of this landslide taken from a chartered helicopter. Photo a) was taken on 3 November, and photo b) was taken on 6 November. The road bridge that can be seen in photo a) was submerged in the landslide-dammed lake in photo b). Both photos clearly showed that the landslide mass was not disturbed through its approximately 100 m distance of rapid movement. As can be seen in photo b), trees on the landslide generally remained straight. However, the forest showed backward rotation at the toe of the landslide (photo a), because the landslide mass filled the Imokawa River and moved upward along the slope of the opposite bank. The building in Fig. 2a was an elementary school. Fig. 2c shows debris that flowed into the entrance and a window of the school building, and mud that scattered onto the building wall. The phenomenon suggested the rapid movement of this landslide. The debris and scattered mud at the school building probably came from a small landslide ("A" in Fig. 2a) at the toe of large displaced landslide mass. This part of the mass did not include the forest, but probably was soils from/around the Imokawa River that was scraped and carried by the displaced landslide mass. Fig. 2d shows a side view of this landslide from which high mobility can be hypothesized based on the angle from the head scarp to the toe of the landslide. The mobilized apparent friction angle was 7.5 degrees.

The toe of landslide climbed up the opposite bank. The height of the lowest part of the landslide-dam crest was raised by piled sandbags that were transported by helicopters of the Japanese Self-Defense Force to prevent overflow of the dam. Standing trees suggested a smooth movement along a liquefied sliding surface. The upper part of the landslide mass was not completely saturated although the sliding surface itself probably was.


Fig. 3 Higashi Takezawa landslide and the head scarp of past landslides (Taken by Sassa)

Fig. 4 Stiff silt (stone) layer outcropped in the head scarp (it inclined around 20 degrees to the landslide moving direction and groundwater flowed over the layer)

Fig. 3 presents another view of the Higashi Takezawa landslide. The head scarp of the current landslide is shown on the figure by red arrows, and the head scarp of the previous landslide is shown by a curved line with red arrows. We investigated the head scarp of this landslide. A very straight, gently-dipping (around 20 degrees) stiff silt (stone) layer outcropped as shown in Fig.4. This layer seemed to be a part of sliding surface of this landslide. It is relatively impermeable and groundwater flowed over this stiff silt layer. The sand layer over this stiff silt layer was soft. It was probably a part of previously moved landslide mass. A sample (H2) was taken from this sand layer behind the current sliding surface as seen in Fig.5.

Fig. 5 Sampling from the sand layer behind the sliding surface and over the stiff silt (stone) layer

Three days after (26 October 2004) the earthquake, an air borne laser scanning survey was conducted, and Fig. 6a presents its result. The gentle slope found in the contours clearly presented the previous landslide topography above the head scarp of this landslide. The central section A-A of the landslide is presented in Fig.6b that includes an interpretation of landslide process based on the topographical map made by the air borne laser scanner after the landslide, the 1/25000 topographical map before the landslide, and field observations. In Fig. 6b, the black line presents the ground surface before the landslide, and the green line shows the ground surface after the landslide. The mass A (red dots) and the mass B (black dots) are the unstable mass before the current landslide movement.

The initial average slope angle between P1 and P2 is around 14.6 degrees, and the average slope angle between P1 and P3 is around 13.5 degrees. The mobilized energy line between P1 and P4 (highest point) is around 7.5 degrees. Hence, this rapid landslide occurred in a gentle slope less than 15 degrees, and the mobilized average apparent friction angle during motion was 7.5 degrees. The large difference between the energy line and the center of gravity of the moving mass suggests a rapid motion.

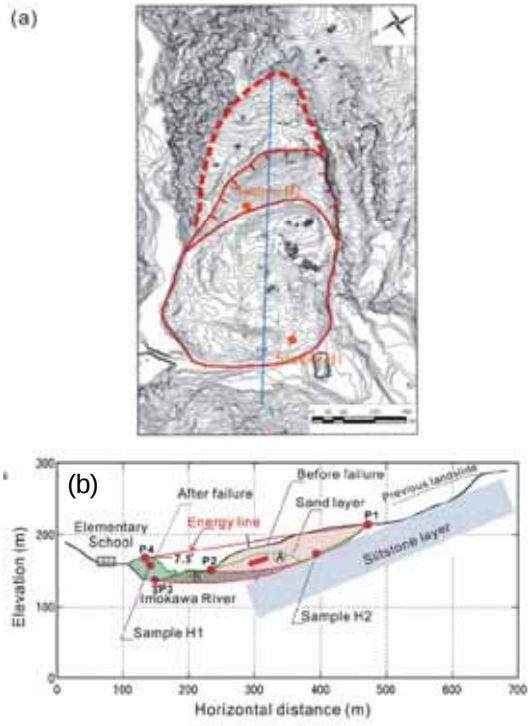


Fig. 6 (a) Plan of the landslide (the map was made by the air borne laser scanning in the courtesy of Aero Asahi Corporation. Contour lines are 2 m spacing); (b) Section of the landslide along A-A line in Fig. 6a

For this landslide, the first question arose on the position of sliding surface from this observation. The outcropped silt (stone) layer was very stiff and apparently too strong to slide. However, the silt near the border to the sand layer could be soft due to weathering because an adequate groundwater flow existed. Accordingly there are two options for the location of sliding surface of this outcropped head scarp, 1) weathered top part of lower silt layer, 2) bottom of upper sand layer. This will be examined later in this paper based on the dynamic loading tests and detailed section.

The second question arose on the sequence of landslide movement. There are two possible scenarios. 1) Block B was firstly liquefied, then the block A started to move due to loss of support in its toe, 2) Block A initially started to move due to seismic loading and the resulted excess pore pressure generation. Thus, the movement of block A then gave an undrained loading to block B. This undrained loading effect can be greater than earthquake loading for the Block B. Then, the block B started to move with the block A and crossed the Imokawa River and hit the opposite bank. Block B is near the river water, and the lower half of this mass was apparently continually submerged under the groundwater. Such part was deoxidized and became blue or gray in color, while the oxidized parts are brown. The deoxidized gray color sand was found on the opposite bank and around the school (into which some part of soils entered).

Pore pressure generation on the shear surface in crushable sands is greatly affected by shear displacement (Wafid et al 2004, Sassa et al 2004). Block A is loaded by shear stress due to self weight and seismic loading. Block B is loaded almost exclusively by seismic loading due to its flat position. Therefore, when the bottom of Block A was saturated, the shear zone should be subjected to greater shear displacement and generate greater pore pressure compared to Block B. There were many terraces along the river, but no liquefaction failure in such terraces near the river was noticed. Another reason is the hardness of sand in this area. The sand is a marine deposit from the Tertiary period. It is much stronger than tuff, pumice or weathered granitic sands, because those sands experienced a long downriver transportation and weaker parts was necessarily removed already through this flow with water. The depth of Block B (around 13 m above the river bed) is much smaller than Block A (around 40 m). Shaking or shearing under a greater overburden pressure could facilitate grain crushing and resulting pore pressure generation. The rapid movement landslides were the cases for more than 25 m in depth such as the Higashi Takezawa landslide, the Terano landslide and the Dainichisan landslide (the biggest landslide in this earthquake). Accordingly, and based on this consideration, it has been concluded regarding the second question that Block A moved firstly due to strong seismic shaking plus the static shear stress due to self-weight of the around 40 m thick soil layer. Therefore, dynamic loading ring shear tests were conducted to simulate the initial movement of Block A.

The Terano landslide (Fig. 7) also formed a landslide dam 4.5 km north of the Higashi Takezawa landslide (Fig. 1). The Terano landslide occurred as landslide blocks in a repeatedly moved residual state. Fig. 7a shows an overview of the Terano landslide, which occurred on a gentle slope; the displaced landslide mass blocked the Imokawa River, forming a landslide dam. This area had been the site of rice paddy fields. Because there was no house or other structure

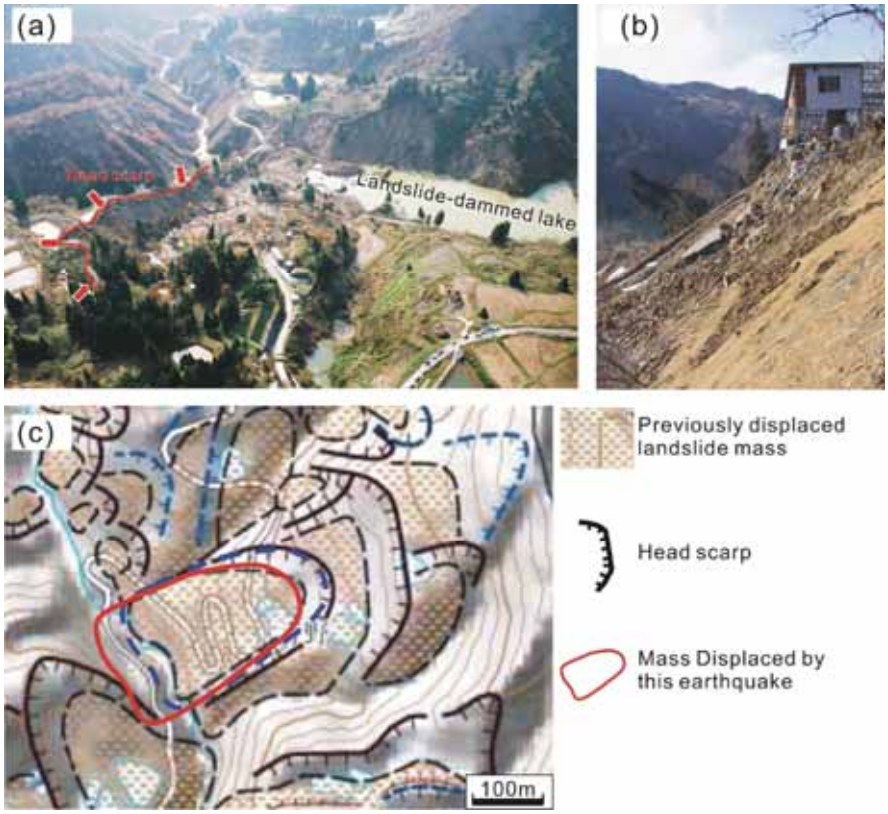


Fig.7 View of the Terano landslide and landslide distribution map of the vicinity. a) Oblique airphoto taken by Sassa on 6 November 2004, b) Side view of the Terano landslide, c) Landslide distribution map and the Terano landslide (Inokuchi et al. 2004)

within the area of the Terano landslide, it was not designated as a landslide risk area. However, the adjacent areas were designated as landslide risk areas. A house stands at the margin of the Terano landslide (Fig. 7b). Fig. 7c shows the location of the landslide mass triggered by the earthquake overlaid on an earlier landslide in a previously made landslide distribution map (Shimizu et al. 2004). In this figure, brown dashed lines define the margins of the previously moved landslide mass identified by airphoto interpretation of the topography. The black dashed lines delineate the head scarps. The blue dashed lines are the main scarp of the landslide before the motion by the Mid-Niigata Prefecture earthquake and the red line presents the landslide block after the movement (Inokuchi et al. 2004).

Fig.8 presents the view from the head scarp to the toe of the Terano landslide. It created a large landslide dam and resulted lake. The landslide is a part of big repeatedly-moving type of landslide complex area, which is typical in the Tertiary mudstone landslide-prone area. Fig. 9a, b show the plan and the section of this landslide. This landslide was also investigated. The main body of the landslide block at the toe was composed of sands (T1) that seem to be similar to the samples of H1 and H2 of the Higashi-Takezawa landslide. In contrast to the Higashi Takezawa landslide, the silt sample (T2) taken from the head scarp was well weathered and soft. The head scarp and Sample T2 was inside the previously moved landslide mass as suggested by the section shown in Fig. 9. The silt was well softened due to landslide motion and well oxidized which was suggested by its brown color. While the siltstone outcropped in the head scarp in the Higashi Takezawa landslide was very stiff and in the stable layer below the landslide mass and probably always saturated suggested by its gray color of deoxidization. The grain size distributions of samples T1, T2 and H2 are shown in Fig.10. Samples H2 and T1 are rather similar though sample T1 includes a slightly greater portion of finer grains. While silt sample T2 is quite different from samples T1 and H2, it is much finer than those sands.

The initial slope angle was 14.9 degrees between P1 and P2 at the top of river bank, and 17.5 degrees between P1 and P3 along the river. The mobilized

average apparent friction angle during motion between P1 and P4 was 12.7 degrees. The difference between the energy line from P1 to P4 and the center of gravity suggests a slower landslide than the Higashi Takezawa landslide.


Fig. 8 Overview of the Terano landslide (Taken by Sassa on 6 November 2004)

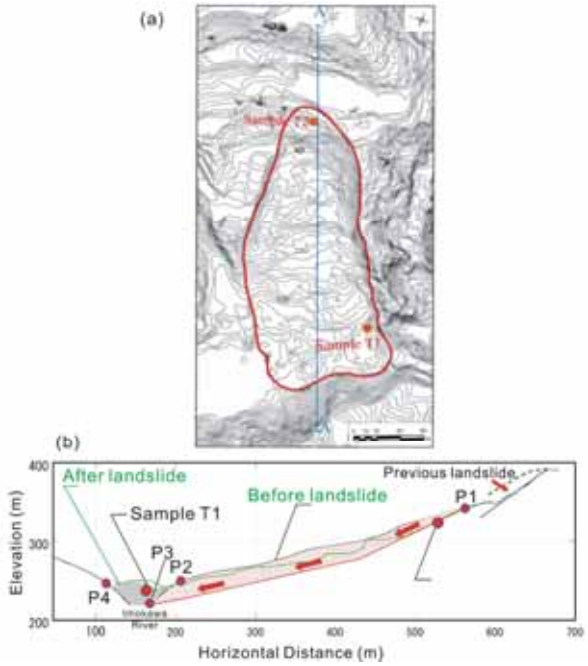


Fig. 9 Plan and Section of the Terano landslide (a: Plan obtained from air bone lazar scanner. Contour lines are 2m pitch. b: Central section A-A of the Fig.9a)

The largest landslide in area and volume triggered by the Mid-Niigata Prefecture earthquake was the Dainichisan landslide (Fig. 11), which is located 1 km west of the Higashi Takezawa landslide (Fig. 1). As indicated in Fig. 11a, the Dainichisan landslide is a typical slump. This landslide did not reach the Imokawa River, and thus did not cause a landslide dam. Fig. 11b shows the exposed probable sliding surface, which is an inclined siltstone bed.

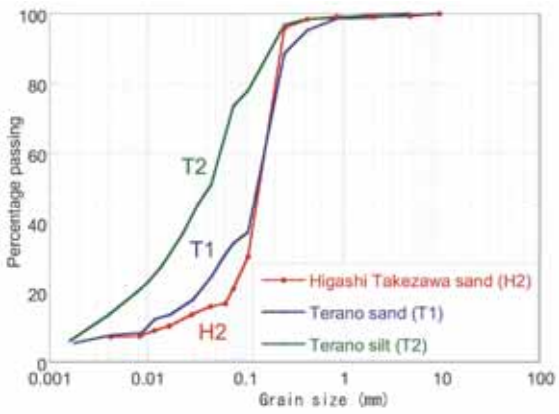


Fig.10 Grain size distribution of three collected samples

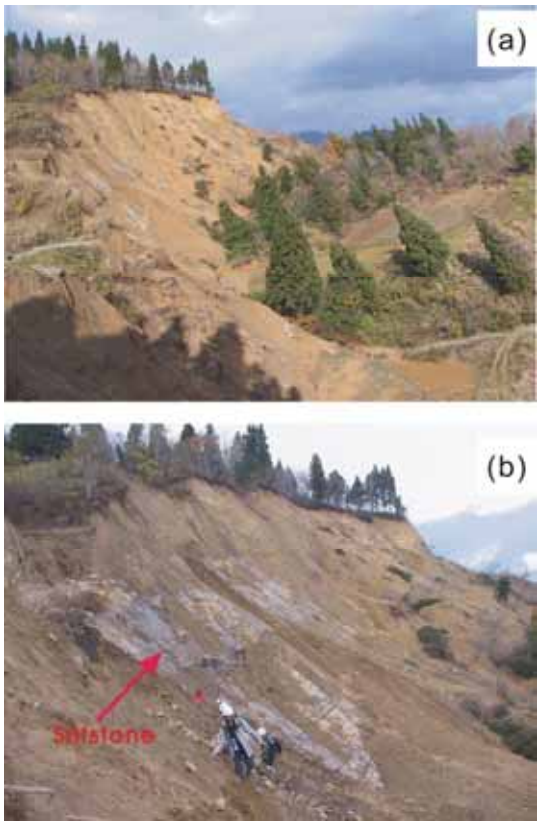


Fig. 11 Dainichisan landslide (a) and head scarp (b)

Sand covered the siltstone bed. Almost all of the large landslides triggered by the Mid-Niigata Prefecture earthquake occurred in this sand layer and/or a silty sand or silt layer. Whether the sliding surface formed at the bottom of the sand layer or at the top of the siltstone is in question. The situation was the same for the Higashi Takezawa landslide.

The Higashi Takezawa, Terano and Dainichisan landslides were 25-50 m deep-seated landslides. The Haguro landslide (Figs. 1, 12a) was relatively shallow, and the landslide mass was very disturbed because of

the steep slope and its shallow depth. This landslide destroyed a road and many parked cars, but fortunately no one was killed. The relatively small rock slide in the Myoken area (Fig. 12b) covered a main road and buried a car occupied by a mother and two children. The rescue team noticed the car buried under the displaced landslide mass, and tried to rescue the occupants. However, the rescue operation took three days because of the very unstable landslide rock debris. The rescue activities were monitored and broadcasted every day by TV and other media. Finally a 2-year-old boy was safely extracted from the buried car. The Myoken landslide occurred on a convex slope. In addition, it was dry, which was one reason the boy could survive for 92 hours under the landslide mass.


Fig. 12 Oblique airphoto of the Haguro landslide (a) and the Myoken landslide (b). Both photos were taken from a helicopter by Sassa on 6 November 2004.

### 3. Influence of rainfalls in prior to the earthquake

The Mid-Niigata Prefecture earthquake in October 2004 occurred 3 days after 100 mm of rainfall was triggered by typhoon No.23. Its effects differed from those of the Hyogoken-Nambu earthquake, which occurred in the dry season (January) of 1995 when there was no rain immediately prior to the earthquake. The Hyogoken-Nambu earthquake was M7.2 and its epicentral depth was 17 km. The Mid-Niigata Prefecture earthquake was M6.8 with an epicentral depth of 13 km. Thus, the earthquake energy was smaller in the Mid-Niigata Prefecture earthquake than in the Hyogoken-Nambu event, but the number and scale of landslides were much greater in the Mid-Niigata Prefecture earthquake. 362 landslides with a width of more than 50 m and 12 large-scale landslides with volumes of more than 1 million cubic meters were triggered by the earthquake (Ministry of Land, Infrastructure and Transport 2005), while the only remarkable landslide triggered by the Hyogoken-Nambu earthquake was the Nikawa rapid landslide (volume of 1.1-1.2 x $10^5$ $m^3$ and a width of 125 m), which killed 34 peoples (Sassa et al. 1996; Sassa 1996). A possible reason for this difference was the influence of rainfall in prior to the Mid-Niigata Prefecture earthquake.

The Japan Meteorological Agency uses the so-called Soil Water Index (SWI) as an index to evaluate the water stored beneath the surface of the ground (Okada 2001). Fig. 13 illustrates the concept of the SWI. SWI is an effective technique for estimating the landslide disaster potential by comparing the values of Soil Water Index for past landslide disasters. SWI uses the Radar-AMeDas (name of radar system for precipitation monitoring) precipitation analysis as an input rain value for the three steps of a serial storage tank model to express water runoff to the ground surface, the surface soil layer, and the deeper soil layer. This model expresses the shift of rain to the ground water with time delay (Ishihara and Kobatake 1979). The groundwater will be stored in each tank corresponding to different soil layers. SWI is defined to be the total storage thickness of the three tanks. The index value is decided for each 5 km×5 km cell. For Japan, number of cell in the mesh is 14,132.

SWI can establish a suitable standard for each 5 km × 5 km cell based on the record of past landslide disasters and amount of precipitation prior to the events. When the record of landslide disasters is not available, SWI can present the extent of danger based on the ranking of SWI value in the past 10 years by quoting the past ten years historical ranking value among its surrounding meshes in which landslides occurred.

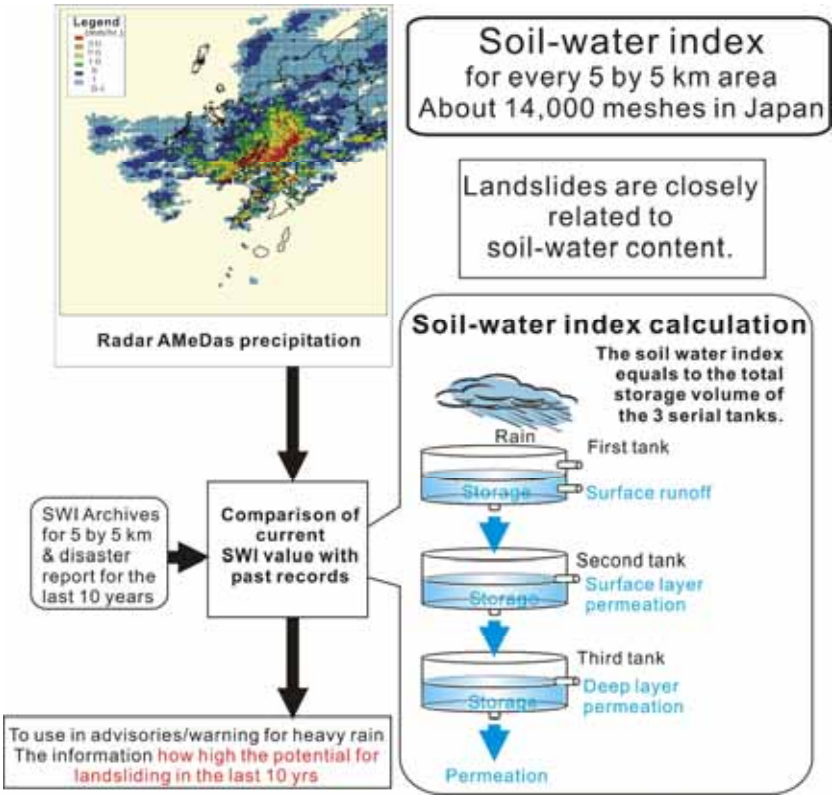


Fig. 13 Soil Water Index (SWI) used by the Japan Meteorological Agency. Height of the upper outlet in the first tank is 60 mm, and the height for the other outlet in the first tank, second tank and third tank is 15 mm.

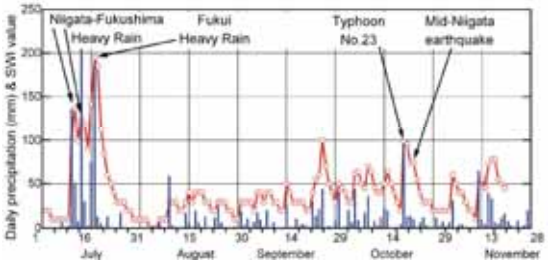


Fig.14 Time sequences of SWI at Yamakoshi Village from July 1st to Nov. 20, 2004 (Rainfall in blue; SWI in red.)

As an example, the present SWI in a certain area showed the highest value (1st rank) in the past 10 years or 2nd highest value within the past 10 years. Landslide disasters occurred in the 1st and 2nd rank of SWI in the neighboring areas. Therefore, caution and preparedness is necessary for possible landslide disasters.

As a result of SWI analysis for landslides that occurred from 1991 to 2000:

- About 60 percent of the landslide disasters occurred in the areas with 1st rank historical rain, both multiple rain areas and light rain areas.
- Most of the large-scale landslide disasters occurred in 1st rank historical rain.
- More than 80 percent of landslides with fatalities occurred in 1st rank historical rain.

Thus, when 1st rank SWI value in the past 10 years is recorded for a certain city, the heavy rain warning of "The danger of landslide disaster for this city is the highest in past several years" is announced. The effect of the historical ranking of SWI is confirmed by the fact that 96 percent of large-scale landslides occurred in the cities of its 1st rank of SWI appeared in Niigata prefecture during 2004 Niigata heavy rain.

Fig. 14 shows the time sequences of SWI at Yamakoshi Village from July 1 to November 18, 2004. During 2004 many heavy-rain events struck Japan, and some of these heavy rains occurred at Yamakoshi Village, resulting in major landslide disasters. For the Niigata-Fukushima Heavy Rain from July 10 to July 14, the total amount of rain recorded by Rader-AMeDas Precipitation was 428 mm, and the maximum index value was 124 at July 13, 1900 hrs. For the Fukui Heavy Rain from July 16 to July 18, total amount recorded was 272 mm by Rader-AMeDas Precipitation, and the maximum index value was 195 at July 17, 2000 hrs. The past maximum index value during 1994 to 2003 was 142. So the maximum value in this area was exceeded in 2004.

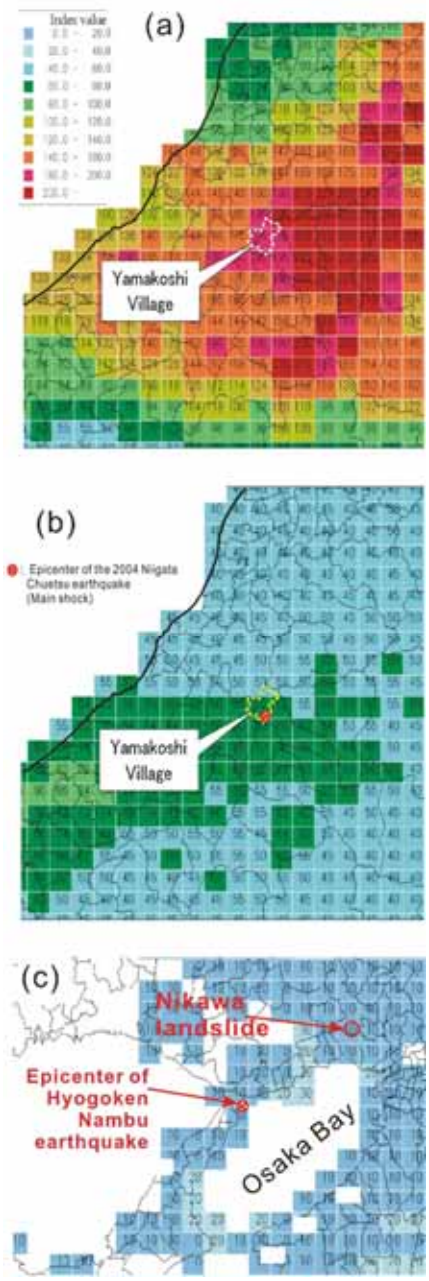


Fig. 15 SWI distributions in Yamakoshi Village and in the Osaka-Kobe area. (a) SWI distribution (Fukui heavy rain) from 16-18 July 2004 in the vicinity of Yamakoshi Village, (b) SWI distribution on the day of the Mid-Niigata Prefecture earthquake (23 October 2004) in the vicinity of Yamakoshi Village, (c) SWI distribution on the day of the Hyogoken-Nambu earthquake on 17 January 1995 in the vicinity of the Nikawa landslide.

However, large landslides did not occur in this period of heavy rain. The parameters of the tank model were decided based on monitoring of the granitic slopes. Granitic slopes that have suffered from many previous landslides during heavy rains have greater permeability than slopes in the Tertiary weathered mudstone area of Niigata. Thus, reconsideration of the rainfall parameters is necessary. Landslides in the mudstone area of Niigata often activate during the snow-melt season. Long-term precipitation is effective for causing landslides in this area rather than short-term precipitation probably because of the low permeability in the mudstone layer.

After these heavy rains, the SWI reached zero in August and thereafter the value was around 20-40. However, typhoon No. 23 on 20 October renewed the heavy rainfall in this area. Three days after the typhoon, the Mid-Niigata Prefecture earthquake occurred. At that time, SWI value was 62, a high value in this area except for the two extraordinarily heavy rains in July.

Fig. 15 presents the SWI distribution in the area including Yamakoshi Village during the Fukui heavy rain (highest SWI value in history) and during the Mid-Niigata Prefecture earthquake, and the SWI for in the area including the Nikawa landslide, which killed 34 persons during the Hyogoken-Nambu earthquake. The SWI values were quite different in the Hyogoken-Nambu earthquake and in the Mid-Niigata Prefecture earthquake; however, the geology in the two areas was somewhat different.

234 landslides more than 50 m wide occurred in the Mid-Niigata Prefecture earthquake, while the Nikawa landslide (more than 125 m wide) was only the large landslide with long travel distance in the Hyogoken-Nambu earthquake. This large difference was likely caused by the heavy rainfall prior to the Mid-Niigata Prefecture earthquake. The combined effects of rainfall and earthquakes are necessary to be studied in landslide risk evaluation for the earthquake-rainfall complex landslide disasters.

## 4. Urgent response to prevent disastrous failure of landslide dams

More than 50 landslide dams were formed along the main channel of the Imokawa River and its tributaries by the landslides triggered by the Mid-Niigata Prefecture earthquake. Because of their size, the two most critical landslide dams were the Higashi Takezawa landslide dam and the Terano landslide dam. Both of these landslide dams were about 350 m long and had volumes of more than 1 million $m^3$.

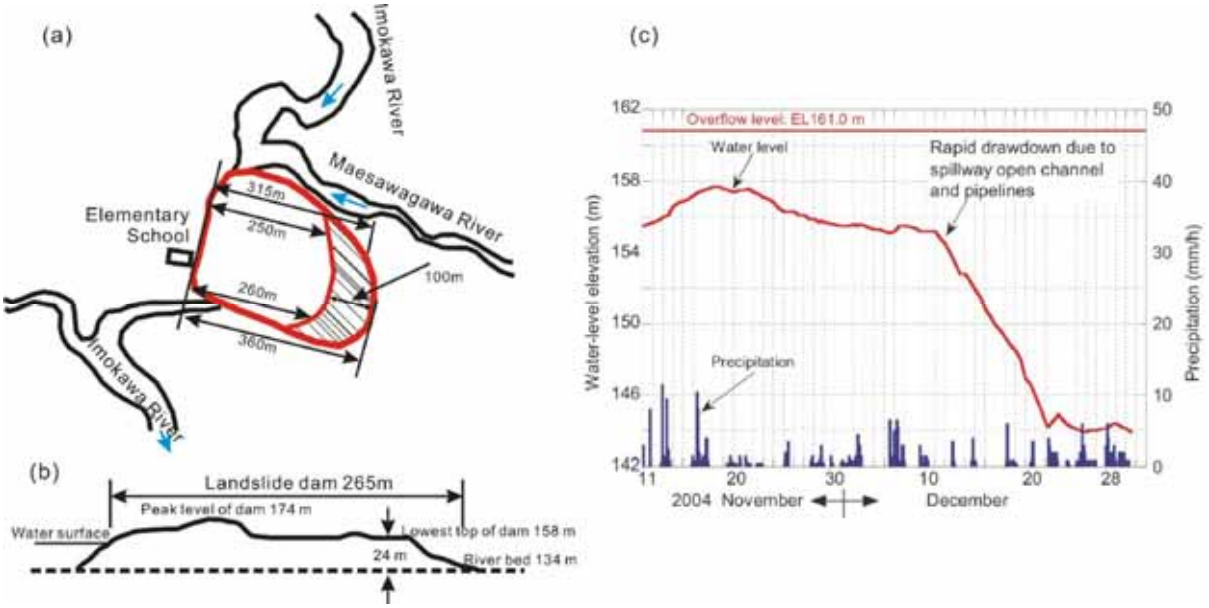


Fig. 16 View (a) and cross section of the Higashi Takezawa landslide dam (b) along the Imokawa River, and elevation of the water level in the landslide-dammed lake (c)

In both cases, the length of the buried river channel was about 10 times the maximum water depth of the lake. Therefore, the possibility of the destructive collapse of either dam by water pressure and/or piping was estimated to be low.

However, there remained the possible danger of overtopping and successive breaching of one or both dams. Failure of these landslide dams could cause outburst floods or debris flows which would endanger downstream residential areas and roads. Therefore, the inhabitants of the downstream area would have to evacuate. It was urgently necessary to lower the level of the landslide-dammed lake. Emergency measures to prevent failure of the landslide dams were carried out by the Ministry of Land, Infrastructure and Transportation with the cooperation of the Self-Defense Force (Marui 2004). The Higashi Takezawa, the largest landslide dam, which is located farthest downstream among five main landslide dams along the Imokawa River, impounded a lake that was critical. Fig. 16a, b presents the plan and the cross section of the Higashi Takezawa landslide. The width of this landslide was 265 m, and its peak elevation was 174 m. The elevation of the lowest part of the dam crest was 158 m, and the river-bed elevation was 134 m. In order to reduce the danger of overtopping, various emergency measures were undertaken. As a result, the lake level was kept lower than the overflow elevation of 161 m, and lake level was lowered to a safer level, as shown in the figure of monitored water-level elevation and precipitation through the end of 2004 (Fig.16c).

Fig. 17 shows photos of some of emergency measures. The Japanese Self-Defense Force transported sand bags to shift up the overflow level by 3 m from the low point of the crest at 158 m to the top of the sand bags at 161 m (Fig. 17a). Then, the water level was lowered by means of pumps and siphons. Twelve pumps were installed. As the result, the monitored water level was kept lower than the overflow level at elevation 161m. It is not suitable to use drainage pumps for the long term; thus, they should be used for only emergence purposes in the initial stages. Because of maintenance problems for the pumps, alternative diversion pipelines (Fig. 17b) were installed to prevent overtopping. These additional diversion pipelines were quite effective. Finally, an open channel (Fig. 17c) with a sufficient cross-sectional area for water discharge including snowmelt during early spring was constructed. It was absolutely necessary to retain the stability of the earthquake-induced landslide against secondary motion during construction of the channel. Therefore, excavation of the upper part of the displaced soil mass was immediately carried out as an appropriate emergency countermeasure. Monitoring on secondary displacement of the landslide was also carried out for security during the construction works.


Fig. 17 Emergency measures to prevent failure of the Higashi Takezawa landslide dam. (a) Helicopters of the Japanese Self-Defense Force carried sandbags and piled them on the lowest part of the landslide dam crest every several minutes during our observation, (b) and (c) Diversion pipe lines and open-channel spillway constructed by the Ministry of Land, Infrastructure and Transportation

## 5. Landslide dynamics tests

To investigate the dynamic properties of two earthquake-induced rapid landslides, dynamic (seismic and cyclic) loading ring shear tests were conducted by DPRI-5 apparatus, one of five dynamic-loading ring-shear apparatuses (DPRI-3,4,5,6,7) developed in DPRI, Kyoto University (Sassa et al. 2003 and 2004). The size of sample box in donuts shape is 120 mm in inside diameter and 180mm in outside diameter, the maximum shear speed in the center of sample is 10 cm/sec, maximum frequency of cyclic loading is 5 Hz, and the maximum rate of data recording is 200 readings/sec.

### 5.1 Real earthquake wave loading test for the Higashi Takezawa sand (H2)

Seismic loading test was performed to simulate the initiation of the Higashi Takezawa landslide using the real monitoring record of the Mid-Niigata earthquake in the closest site. The monitored record is from one observation station of K-NET (Kyoshi Net), which is the strong earthquake motion monitoring network by the National Research Institute for Earth Science and Disaster Prevention (NIED). K-NET is a system which sends strong-motion data on the Internet. The data are obtained from 1,000 observatories (25 km mesh) deployed all over Japan. The nearest monitoring site to the Higashi Takezawa landslide is the observation station of NIG019 at Ojiya, around 10 km west of the Higashi Takezawa landslide, and WNW 7 km from the epicenter of the main shock. The Higashi Takezawa landslide is ENE 3.6 km from the Epicenter. The location of the epicenter is between the NIG019 and the Higashi Takezawa landslides, but closer to the landslide.

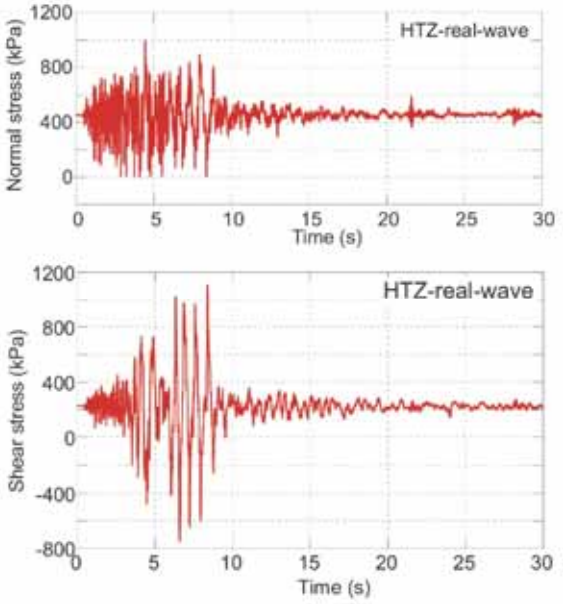


Fig. 18 Normal stress and shear stress during the Mid-Niigata earthquake working on the sliding surface of the Higashi-Takezawa landslide, which was calculated from the monitored earthquake record at the monitoring site NIG019 in K-NET (NIED)

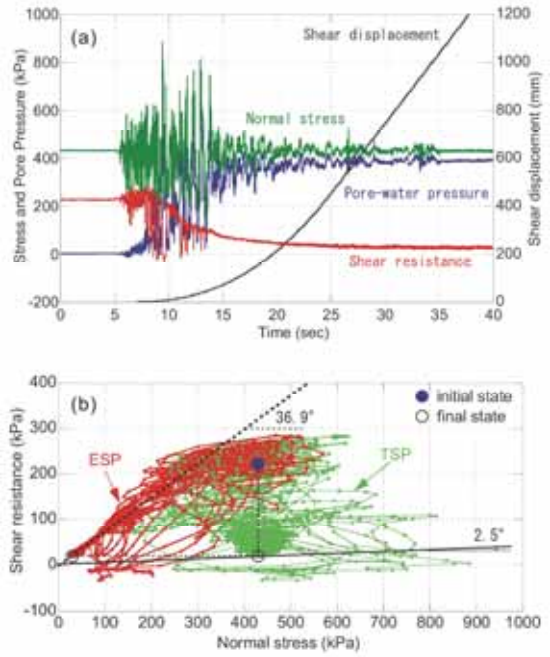


Fig.19 Undrained real earthquake wave loading test to simulate the Higashi-Takezawa landslide ($B_D$=0.98). (a) Time series data, and (b) Stress path

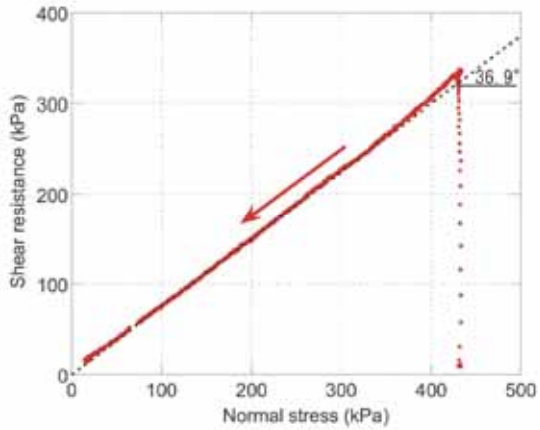


Fig.20 Stress path obtained in the drained constant speed test after the real wave loading test (Fig.19)

The real acceleration and its wave form that affected the Higashi Takezawa landslide can not be known in detail as it is complex due to inter alia topography, geology, underground structure, and distance from the fault and the epicenter. Therefore, the monitored earthquake record in NIG019 was applied as the first approximation of input acceleration to the sliding surface. Using three components of acceleration records, normal stress component and shear stress component on the bottom of landslide were calculated based on the section of the Higashi Takezawa landslide.

The test procedure is as follows. The sliding surface is approximated as the one dimensional slope (20 degrees and 40 m deep, and a half of the layer was saturated, namely groundwater level was 20 m deep). The total density of soil layer was assumed to be 1.8 $Mg/m^3$. Sample H2 was placed dry into the shear box and saturated by firstly replacing pore air by $CO_2$ gas and then replacing $CO_2$ by de-aired water. The pore pressure parameter ( $B_D = \Delta u / \Delta \sigma$ ) was measured as the confirmation of full saturation ($B_D$ = 0.98). Then, the shear stress before the earthquake on the sliding surface of 230kPa was loaded under drained conditions. Thereafter, the shear box was shifted to the undrained state by closing the drainage valve, and then the calculated seismic stresses were applied. The data is shown in Fig.18. The result of seismic loading of the sample was presented in the time series monitoring result of loaded normal stress, mobilized shear resistance (not the same with the applied shear stress because failure occurred in the sliding surface at the failure line), generated pore pressure and the resulting shear displacement as seen in Fig.19a. Due to seismic shaking, pore water pressure was generated, then shear failure occurred and shear displacement started. As shear displacement progressed, a typical sliding surface liquefaction phenomenon was produced (Sassa 1996, Sassa 2000, Sassa et al 2004), namely grain crushing along the shear zone proceeded and a higher pore pressure was generated in progress with shear displacement. The sand was originally a marine deposit and much stronger than volcanic deposits such as pyroclastic flow deposits and pumice, and also weathered granitic sands. However, the shearing stress under 40m overburden pressure is enough to cause grain crushing and resulting volume reduction. It caused sliding surface liquefaction. The mobilized apparent friction angle is only 2.5 degrees at the steady state. The stress path of the test is shown in Fig.19b (in which a red color stress path expresses the effective stress path and a green color stress path presents the total stress path). The apparent friction angle is obtained from the ratio of mobilized steady state shear resistance divided by initial normal stress. The effective friction angle mobilized in the post failure process is not so clear in Fig.19b. So after this test, pore pressure was dissipated by opening the drainage valves. After full dissipation, sample was sheared under the speed control condition at 0.2 mm/sec. Normal stress was reduced at the unloading rate of 0.5 kPa/sec after

reaching the peak shear resistance. The failure line mobilized in the post failure process (residual state) gave 36.9 degrees for the friction angle (Fig.20).

In addition, a series of cyclic loading tests to compare the dynamic properties of the sand H2 of the Higashi Takezawa landslide and the sand T1 of the Terano landside, and the silt T2 of the Terano landslide were conducted.

### 5.2 Cyclic loading test for the Higashi Takezawa sand (H2)

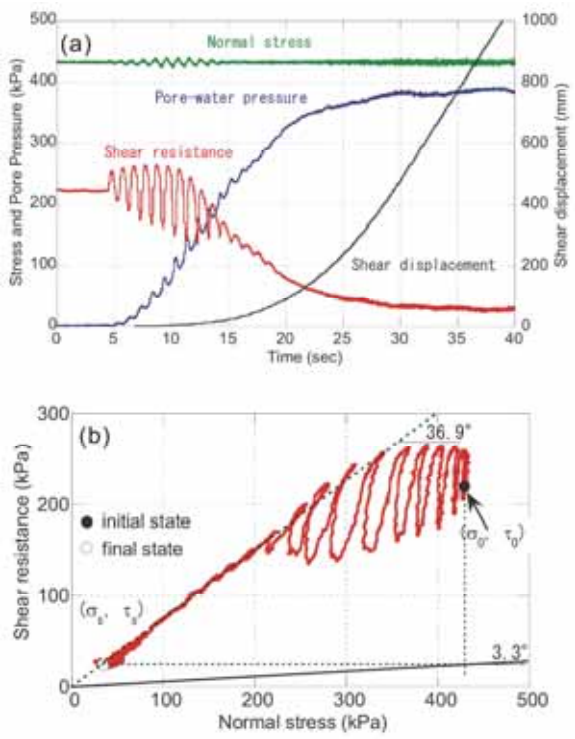


Fig.21 Undrained cyclic loading test of the Higashi Takezawa sand (H2) ($B_D$=0.98). (a) Time series data, and (b) Stress path

For sample H2, the sample preparation and test condition were the same with the above mentioned test. The main differences were the loading stress, frequency and wave form. During the test, normal stress was kept constant, because the effective normal stress practically would keep constant in the fully saturated undrained condition when subjected to any change in the normal stress. Shear stress with the wave form of sine curve at 1 Hz frequency was applied. To ensure the failure, the shear stress was increased step by step until 15 cycles. The test result for the Higashi Takezawa sand is presented in Fig.21.

The sample was subjected to the sliding surface liquefaction as that shown in the real wave seismic loading test. The mobilized apparent friction angle at the steady state is 3.3 degrees, almost the same level with that shown in Fig.19b. The failure line estimated from the effective stress path in the post failure stress path is 36.9 degrees, see Fig.21b.

### 5.3 Cyclic loading tests for the sand (T1) and silt (T2) of the Terano landslide

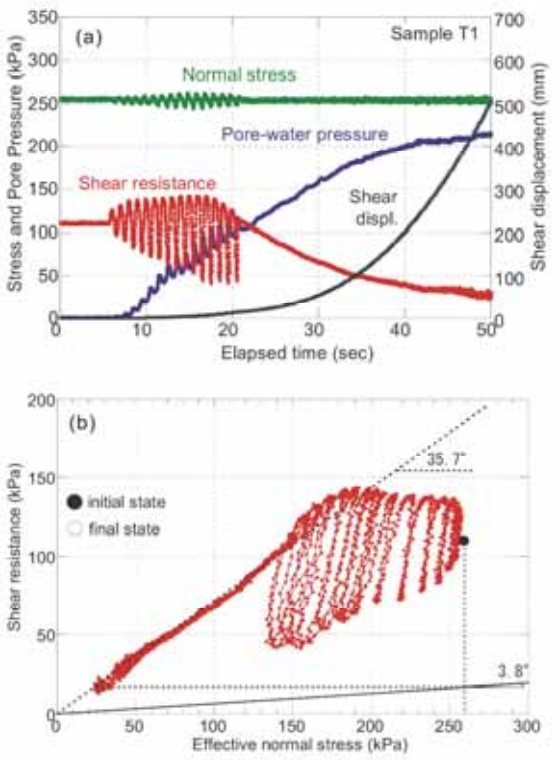


Fig.22 Undrained cyclic loading test on the Terano sand (T1) ($B_D$=0.98). (a) Time series data, and (b) Stress path

The slope angle of the ground surface of the Terano landslide is 17.5 degrees at average from the toe of the slope at the Imokawa River (P3) to the top of head scarp (P1) in Fig.9b. The slope condition for the cyclic loading test was approximated as a 17 degree slope with the depth of landslide mass above the sliding surface being 20 m. Around half of the landslide mass was assumed to be saturated, namely the groundwater table was assumed to be 10 m deep from the ground surface.

During the test, normal stress was kept constant, and shear stress of sine curve of 1 Hz loading frequency was applied. The shear stress was increased step by step until 15 cycles. All test conditions were the same for T1 sand and T2 silt.

The cyclic loading test result for the Terano sand (T1) is shown in Fig.22. The Terano sand was clearly subject to sliding surface liquefaction after failure. The mobilized apparent friction angle at the steady state is 3.8 degrees, slightly greater than H2 (2.5 degrees in Fig. 19b, and 3.3 degrees in Fig. 21b). The mobilized effective friction angle that is estimated from the stress path after the peak is 35.7 degrees, about one degree less than the 36.9 degrees for the Higashi Takezawa sand. This may be due to the fact that the Terano sand is slightly finer than the Higashi Takezawa sand as found in Fig.10. However, the both sands are generally similar.

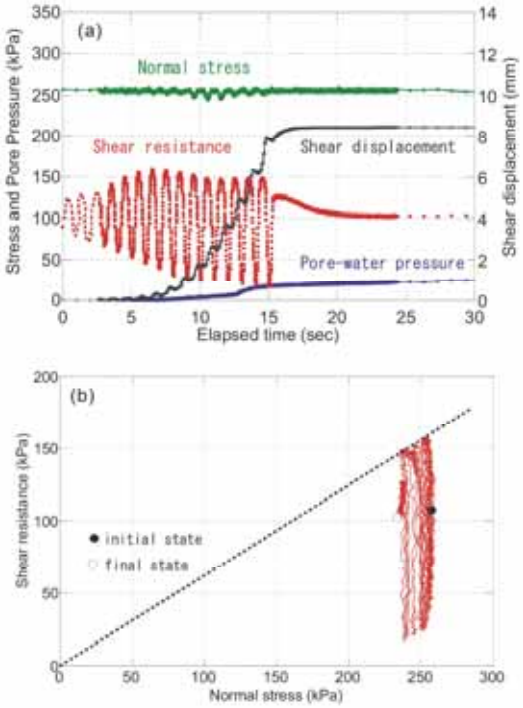


Fig. 23 Undrained cyclic loading test on the Terano silt (T2) ($B_D$=0.98) (a) Time series data, and (b) Stress path

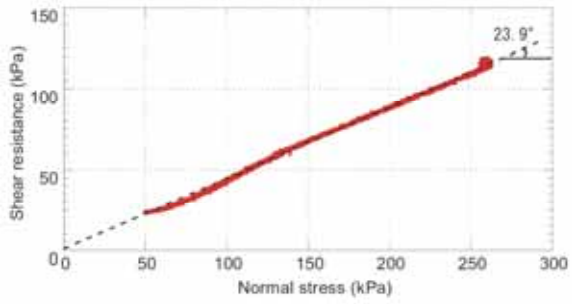


Fig.24 The residual state of friction angle for Terano silt (T2)

The results of cyclic loading test on the Terano silt (T2) is presented in Fig. 23. The dynamic properties of the Terano silt are quite different to the sands. The sliding surface liquefaction and its resulting rapid landslide motion were not produced in this test. Shear displacement was increased only during the cyclic loading, precisely say, only in the time span when the loaded stress reached or exceeded the peak shear strength. It was the repeated movements of stop and move, and the shear movement stopped at the same time with the final cycle of loading. High pore pressure was probably not generated or at least not monitored as seen in Fig.23a.

To obtain the effective friction angle in the residual state or the post failure condition, the sample was sheared at a constant shear speed of 0.05 mm/sec by using the shear-speed-controlled method, while the normal stress from was increased from 50 kPa to more than 250 kPa at a loading speed of 0.1 kPa/sec in the drained condition. The residual friction angle was 23.9 degrees for the friction angle (Fig.24). The friction angle was 13 degrees less than the Higashi Takezawa sand, and around 12 degrees less than the Terano sand. The silts and sands display quite different shear characteristics.

**6. Solution for the first question**

In the Higashi Takezawa landslide, a stiff silt (stone) layer outcropped in the head scarp. And a very similar stiff silt (stone) layer outcropped in the Dainichisan landslide (Sassa et al. 2005). Therefore, whether the location of sliding surface is formed on the weathered part of silt or on the bottom of sand layer is of great importance for understanding the triggering mechanisms of these landslides. The weathered part of silt can not be found, probably it is very thin. However, weathered silt (T2) was taken in the Terano landslide.

The effective friction angle is 12-13 degrees less than the sand. It means a landslide should occur in the silt layer when rain or melting snow is the triggering factor of landslides. This area is known as a Tertiary mud stone landslide area. Many landslides cover this area (Shimizu et al. 2004 or NIED Web page for landslide map).

The area of Niigata Prefecture is known as a heavy snow area and snow melt is the usual main source of water supply for the ground. Slow and limited shear displacement is the common form of movement of

landslides here. In the case of water supply due to snow melting or long rain, it is certain that silt is much weaker than the sand. Therefore, previous landslides probably occurred at the sliding surface in the silt layer, most likely in the weathered part of silt just below the sand layer. In contrast, the silt is strong against the earthquake, while sand is weak against earthquake loading. Sand grains are much easy to crush and susceptible for volume reduction. Therefore, earthquake induced landslides should form its sliding surface within sand. The dynamic loading ring shear tests indicate that the most likely scenario to cause the Higashi Takezawa and the Terano landslides was one in which the sliding surface liquefaction phenomenon occurred within the sand layer under a high overburden pressure.

## 7. Landsliding simulation of Higashi Takezawa landslide

A geotechnical landslide simulation model was proposed by Sassa 1988. It was improved to a computer code for general use during APERITIF project especially in the data input and three-dimensional presentation of output. This new computer code for rapid landslides (Rapid/LS) was applied to simulate the motion of the Higashi-Takezawa landslide. In addition to the steady-state shear resistance which can be measured with ring-shear apparatus, another parameter for geotechnical simulation, the lateral pressure ratio $K$ was introduced to express softness or potential for lateral spreading of the moving mass. According to the parameter, the lateral pressure acting on a soil column is close to 1.0 if the material appears to be liquid. Liquid spreads laterally without limitation on the flat plane. In contrast, if the material is completely solid (like metal or a rock mass), the lateral pressure ratio $K = 0$. A hard rock can stand on the plane and never spread laterally. Soils are in between. It will be reasonable to assume that the value inside a moving soil mass will be between 0 and 1, though the lateral pressure ratio in the static soil mass can be more than 1.0 under the over consolidated state.

In the case of Higashi-Takezawa landslide, it was assumed relatively lower (0.50–0.65) because the landslide mass was normally less saturated. Shear resistance of the soil sample taken from the sliding zone of the landslide was employed in the simulation.

Figure 25 presents six steps of the three-dimensional visual output of the simulation results from the initial state to the final deposition state. It shows that the sliding mass rushed into the river rapidly, and horizontal flow occurred obviously thereafter.

## 8. Conclusions

1. Two rapid major landslides triggered by the 2004 Mid-Niigata earthquake were investigated. Both created landslide dam on the Imokawa River.
2. Both landslides were initiated within the landslide mass of the previous landslides. The mobilized apparent friction angles of both landslides were 7.1 degrees in the Higashi Takezawa landslide and 12.7 degrees in the Terano landslide.
3. Cyclic loading ring shear test on sands from the Higashi Takezawa landslide and the Terano landslide proved that both sands can be liquefied by the sliding surface liquefaction phenomenon under 20-40 m over burden pressure. While silt taken from the Terano landslide was proved that the silt was not subjected to high pore water pressure generation by cyclic loading, and the shear displacement was only limited when the shear stress reached or exceeded the failure line, the movement stopped at the end of cyclic loading.
4. On the contrary, the effective friction angle of silt is 23.9 degrees, smaller than those of sands (36.9 degrees and 35.7 degrees). Therefore, landslide movement due to snow melting or rainfalls should have its sliding surface in the silt layer. It is estimated from these test results that previous landslides in both areas probably slid in the silt layer; however the rapid landslides triggered by the 2004 Mid-Niigata earthquake formed their sliding surface within the sand layer.
5. A dynamic loading ring shear test to simulate the Higashi Takezawa landslide using the monitored seismic record in Ojiya (NIG019) on the sand collected from the head scarp of the landslide reproduced the initiation of rapid landslide resulting from the sliding surface liquefaction. The mobilized friction angle at the steady state was only 2.5 degrees.

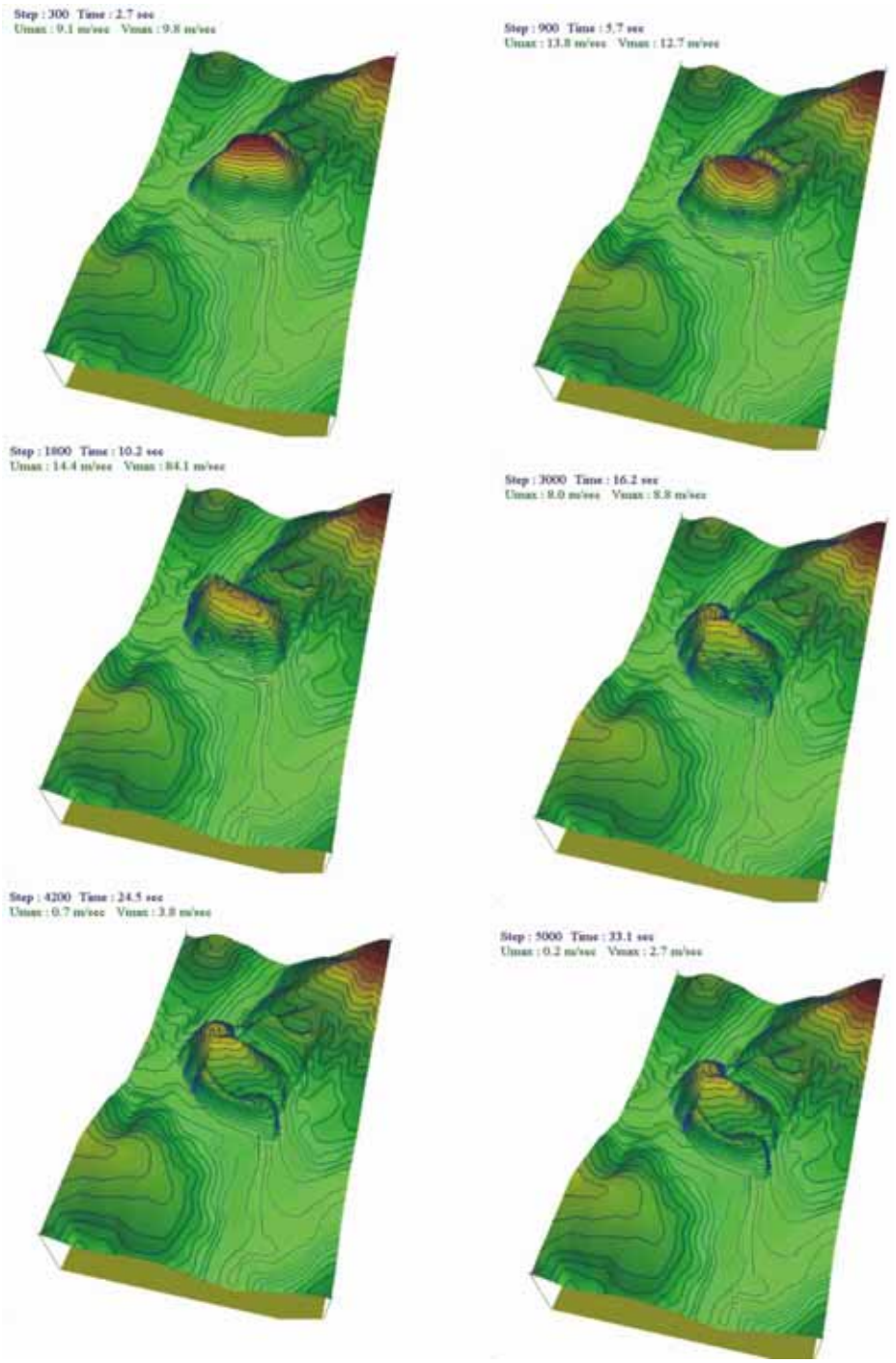


Fig. 25 Simulation results on the Higashi-Takezawa landslide

**Acknowledgment**

This research was conducted as a part of Theme 2: Landslide Investigation of the 2004 Mid-Niigata earthquake disaster investigation by MEXT (Ministry of Education, Culture, Sports, Science and Technology, Japan) Special Coordinating Fund for Science and Technology. The authors acknowledge its special coordinating fund to conduct this investigation and thank all members of this investigation team for discussion. We are grateful for Dr. Gen Furuya and other post-doctoral students and graduate students of the Research Centre on Landslides, Disaster Prevention Research Institute of Kyoto University for cooperation in the field investigation and sampling.

**References**


Chigira, M., Duan, F., Yagi, H. and Furuya, T. (2004): Using an airborne laser scanner for the identification of shallow landslides and susceptibility assessment in an area of ignimbrite overlain by permeable pyroclastics, Landslides, Vol. 1, No. 3, pp. 203-209

Hirata, N., Sato, H., Sakai, S., Kato, A. and Kurashimo, E. (2005): Fault system of the 2004 Mid-Niigata Prefecture Earthquake and its aftershocks, Landslides, Vol. 2, No. 2, pp. 153-157.

Inokuchi, T., Moriwake, H. and Uchiyama, S. (2004): Landslide topography distribution map and a comparison with the landslides triggered by 2004 Mid-Niigata earthquake, Proc. Urgent Symp. Landslide Disaster Caused by 2004 Mid-Niigata Earthquake, pp. 16-25 (in Japanese).

Ishihara, Y. and Kobatake, S. (1979): Runoff model for flood forecasting. Bulletin of Disaster Prevention Research Institute, Kyoto University, Vol. 29, No. 1, pp. 27-43.

Marui, H. (2004): Urgent measures for the mitigation to the possible secondary disaster caused by landslide dams in Higashi-Takezawa and Terano. Proc. Urgent Symp. Landslide Disaster Caused by 2004 Mid-Niigata Earthquake, pp. 114-122 (in Japanese).

Ministry of Land, Infrastructure and Transport (2004): Quick report for Landslides triggered by 2004 Niigata-Chuetsu earthquake. http://www.mlit.go.jp/kisha/kisha04/05/051101_2_.html

Ministry of Land, Infrastructure and Transport (2005): Web information http://www.mlit.go.jp/kisha/kisha05/05/050113_.html

National Research Institute for Earth Science and Disaster Prevention (NIED)(2004): Web of K-Net ttp://www.k-net.bosai.go.jp/k-net/data/

National Research Institute for Earth Science and Disaster Prevention (2004): Web for Landslide map: http://lsweb1.ess.bosai.go.jp/jisuberi/jisuberi_mini/jisuberi_top.html

Okada, K. (2001): Soil water index. Sokko-Jiho, Japan Meteorological Agency, 69-567-100 (in Japanese).

Sassa, K. (1988): Special lecture: The geotechnical model for the motion of landslides. Proceedings of the 5th International Symposium on Landslides, Lausanne, vol.1, pp 33–52.

Sassa, K., Fukuoka, H., Scarascia-Mugnozza, G. and Evans, S. (1996): Earthquake-induced landslides: distribution, motion and mechanisms, Special Issue of Soils and Foundations, pp.53-64.

Sassa, K. (1996): Prediction of earthquake induced landslides, In Landslides, Proc. 7th Int'l Symp. Landslides. Balkema, Rotterdam, Vol.1, pp. 115-132.

Sassa, K. (2000): Mechanism of flows in granular soils, Proc. GeoEng2000, Melbourne, Vol. 1, pp. 671-1702.

Sassa, K. (2005): Landslide Disasters in the 2004 Mid-Niigata earthquake in Japan, Landslides, Vol. 2, No. 2, pp. 135-142.

Sassa, K., Wang, G. and Fukuoka, H. (2003): Performing undrained shear tests on saturated sands in a new intelligent type of ring shear apparatus, Geotechnical Testing Journal, ASTM, Vol. 26, No.3, pp. 257-265.

Sassa, K., Fukuoka, H., Wang, G. and Ishikawa, H. (2004): Undrained dynamic-loading ring-shear apparatus and its application to landslide dynamics, Landslides, Vol. 1, No. 1, pp. 9-17.

Sassa, K., Wang, G., Fukuoka, H., Wang, F., Ochiai, T., Sugiyama, M. and Sekiguchi, T. (2004): Landslide risk evaluation and hazard zoning for rapid and long-travel landslide in urban development areas, Landslides, Vol .1, No. 3, pp: 221-235.

Sato, H., Sekiguchi, T., Kojiroi, R., Suzuki, Y. and Iida, M. (2005): Overlaying landslides distribution on the earthquake source, geological and topographical data: the Mid-Niigata Prefecture earthquake in 2004, Japan, Landslides, Vol 2, No. 2, pp. 143-152.

Sekiguchi, T. and Sato, H. (2004): Mapping of micro topography using airborne laser scanning, Landslides Vol. 1, No.3, pp: 195-202.

Shimizu, F., Oyagi, N., Miyagi, T. and Inoguchi, T. (2004): Landslide Topography Map, Vol. 17 (Nagaoka & Takada area), 1/50,000 and 1/25,000.

Wafid, M., Sassa, K., Fukuoka, H. and Wang, G. (2004): Evolution of shear-zone structure in undrained ring shear tests, Landslides, Vol. 1, No. 2, pp: 101-112.

# 2004年新潟県中越地震により発生した斜面災害について

佐々恭二・福岡　浩・汪　発武・王　功輝・岡田憲治*・丸井英明**

*気象庁
**新潟大学災害復興科学センター

## 要旨

本稿は、2004年新潟県中越地震により発生した斜面災害、地震前の降雨条件及び災害後の復興を紹介すると共に、地すべりダムを形成した東竹沢地すべり及び寺野地すべりを対象に、現地調査及びリングせん断試験を実施し、再活動地すべりにおける地震時高速地すべり発生・運動機構を研究したものである。また、リングせん断試験結果を用いて、崩壊後東竹沢地すべりの運動過程についてシミュレーションを行った。

**キーワード**:地すべり，地震，土壌水分指数，リングせん断試験，運動過程，災害復興